Instability of gravity-driven flow of a heated power-law fluid with temperature dependent consistency

Cite as: AIP Advances **8**, 105215 (2018); https://doi.org/10.1063/1.5049657
Submitted: 24 July 2018 • Accepted: 03 October 2018 • Published Online: 15 October 2018

J. P. Pascal, S. J. D. D'Alessio and M. Hasan

Instability of gravity-driven flow of a heated power-law fluid with temperature dependent consistency

J. P. Pascal,[1,a] S. J. D. D'Alessio,[2,b] and M. Hasan[1,c]
[1]*Department of Mathematics, Ryerson University, Toronto, Ontario M5B 2K3, Canada*
[2]*Department of Applied Mathematics, University of Waterloo, Waterloo, Ontario N2L 3G1, Canada*

(Received 24 July 2018; accepted 3 October 2018; published online 15 October 2018)

In this paper we report on our investigation of the instability of a liquid layer flowing along a heated inclined plane. We develop and implement a theoretical model with a power-law constitutive relation which captures the temperature variation in the rheology of the fluid. We carry out a linear stability analysis and obtain Orr-Sommerfeld type equations for the evolution of infinitesimal perturbations imposed on the equilibrium flow. Numerical solutions were obtained, as well as asymptotic approximations based on the assumption of perturbations of long wavelength and small variation in the consistency of the fluid with respect to temperature. We investigate the critical conditions for the onset of instability and determine the effect of a non-Newtonian rheology and the dependence of the fluid properties on temperature. Nonlinear effects were considered by employing a reduced dimensionality model. Calculations of permanent waves arising from unstable uniform flows were made by carrying out numerical simulations of these equations. https://doi.org/10.1063/1.5049657

I. INTRODUCTION

Gravity-driven flow with a planar free surface is subject to instability due to inertial effects resulting in the formation of waves propagating along the surface. These can have considerable amplitudes with significant impact in many cases related to naturally occurring phenomena and are also of consequence in numerous industrial contexts. The stability of inclined flow is also affected by heating which can cause the occurrence of Marangoni instability. In situations when the inclined flow is heated from below, the resulting thermocapillarity enhances the inertial instability since the associated Marangoni stresses pull fluid from the troughs of surface perturbations toward the crests thus increasing the amplitude. Several theoretical stability analyses, both linear and nonlinear, have been recently undertaken to study the stability of Newtonian flows along heated inclines.[1–4] In these studies the heat transfer from the liquid to the ambient gas is modelled by Newton's law of cooling. This provides a realistic description of real world situations and also allows variation in temperature along the surface thus capturing the occurrence of thermocapillarity.

To establish a more realistic description of nonisothermal flow, one must endeavour to include into the model a dependence on temperature of the fluid properties. Clearly, accounting for a temperature-dependent mass density is important in studying flows where buoyancy is a relevant factor. However, in many such investigations interfacial instability due to inertia is not considered, and the fluid layer is assumed to be horizontal and/or have a non-deformable surface. A recent such example is the work of Hudoba and Molokov[5] who have carried out a linear stability analysis of the buoyancy-driven flow of a heated electrically conducting fluid inside a vertical channel with solid walls in the

[a]email: jpascal@ryerson.ca
[b]email: sdalessio@uwaterloo.ca
[c]email: m.hasan@ryerson.ca

presence of a transverse magnetic field. Goussis and Kelly[6] and Hwang and Weng[7] have incorporated a temperature dependent viscosity in their interfacial instability analysis of inclined flow, however in both investigations the temperature at the free surface is assumed to be prescribed which does not allow for temperature variation and thus negates the Marangoni effect. Recently, Pascal et al.[8] and D'Alessio et al.[9] have implemented a model for film flow with temperature dependent fluid properties which incorporates Newton's law of cooling at the surface.

The basic Newtonian constitutive relation fails to adequately describe a multitude of fluid flows. Such non-Newtonian rheological behaviour is illustrated by various biological fluids, as well as flows involved in diverse industrial processes such as coating applications and the operation of heat exchangers. Cases abound also in geological contexts with examples including lava and debris flows. Theoretical investigations of inelastic non-Newtonian fluids often resort to the power-law constitutive relation due to the fact that it agrees with observations for many real fluids and because, due to its simplicity, it is amenable to detailed analyses. For the isothermal case, the stability of inclined flow of a power-law fluid has received considerable attention from researchers. The general, commonly taken approach is to reduce the dimensionality of the long-wave equations by eliminating the cross-stream coordinate by means of a suitable method. The resulting reduced model lends itself to linear stability and approximate nonlinear, analytical and numerical analyses. Earlier investigations[10–14] have accomplished the reduction in dimensionality by a direct integration of the equations of motion over the depth of the fluid layer. If inertia terms are retained, the resulting model consists of two equations governing the flow rate and the thickness of the fluid layer referred to as the integral boundary layer (IBL) equations. These fail to accurately estimate the critical Reynolds number for the onset of instability, however they adequately predict the size and the propagation speed of the permanent waves that form on the surface of uniformly thick fluid layers under unstable flow conditions. Indeed, the straight integration of the equations approach continues to be used for complicated problems where a more sophisticated dimensionality reduction technique leads to an intractable formulation. For instance, Heining and Aksel[15] have established IBL equations for power-law flow down a nonplanar incline with sinusoidal topography. DiCristo et al.[16] used the IBL model to investigate the formation of roll-waves on gravity-driven flow of power-law liquids. More recently, Iervolino et al.[17] have also resorted to the straight depth-integration approach to obtain a model for power-law flow with substrate filtration.

The deficiency of the IBL equations in predicting the onset of instability was rectified in subsequent studies[18–22] by employing a weighted residual method to eliminate the explicit dependence on the cross-flow coordinate. Amaouche et al.[21] and Ruyer-Quil et al.[22] demonstrated the accuracy of this method by comparing the results with numerical solutions to the Orr-Sommerfeld equations.

Since the power-law model leads to a singularity in the shear-thinning case for vanishing shear rate, an adjustment is required for calculations of inclined flow problems with zero shear prescribed at the surface. Ruyer-Quil et al.,[22] for example, dealt with this issue by introducing a fictitious thin Newtonian fluid layer at the surface. Rousset et al.[23] on the other hand abandoned the strict power-law model and employed the Carreau relation which modifies the power-law formula by introducing an extra parameter. This approach circumvents the singularity, however the formulation is more involved making analysis much more complicated.

The stability of the inclined flow of a power-law film in the non-isothermal case has received surprisingly little attention in the literature. Hu et al.[24] studied the instability of thermocapillary convection in a horizontal layer with a non-deformable surface consisting of a shear-thinning fluid with the rheology described by the Carreau relation. They have included buoyancy effects by assuming a temperature-dependent density. Sadiq and Usha[25] have considered the stability of a power-law flow with constant fluid properties along a heated incline. At the free surface of the film they implement a thermal insulation condition. A more realistic condition, which is implemented in the recent investigations for the Newtonian case, is Newton's law of cooling which allows for heat transfer from the liquid layer to the ambient gas. The insulation condition leads to a depth-independent equilibrium distribution for the temperature in the liquid layer. Consequently, the formation of waves on the surface does not lead to temperature differences and thus does not generate Marangoni stresses. So, if the surface is assumed to be thermally insulated then the model does not capture the enhancement to the inertial instability due to the Marangoni effect.

Recently, Bernabeu et al.[26] have established a model for lava flow consisting of a viscoplastic fluid with a power-law relation for the viscosity. This investigation does not include the Marangoni effect but a temperature dependence is incorporated into the rheological relation.

In the present paper we study the stability of a power-law fluid film flowing down a heated incline. We implement Newton's law of cooling at the free surface and thus take into account the heat transfer from the liquid layer to the ambient gas above. Our theoretical model also allows for variation in the rheology of the liquid with temperature. The paper is set up as follows. In Section II we set up the equations governing the flow. In Section III we obtain an equilibrium solution and apply a linear analysis to study its stability. Nonlinear effects are considered in Section IV, and finally, Section V offers a summary of the conclusions drawn from the entire investigation.

II. GOVERNING EQUATIONS

We consider the two-dimensional flow of a thin liquid film with power-law rheology flowing down an inclined plate heated at a prescribed constant temperature denoted by T_w. The ambient gas is assumed to remain motionless and at a constant temperature $T_\infty < T_w$. A rectangular coordinate system is set up as illustrated in Figure 1. The position of the free surface of the liquid layer is given by $z = h(x, t)$.

Equations of motion are obtained from the conservation of mass and momentum, and can be expressed as

$$\frac{\partial u}{\partial x} + \frac{\partial w}{\partial z} = 0, \tag{1}$$

$$\rho\left(\frac{\partial u}{\partial t} + u\frac{\partial u}{\partial x} + w\frac{\partial u}{\partial z}\right) = -\frac{\partial p}{\partial x} + \frac{\partial \tau_{xx}}{\partial x} + \frac{\partial \tau_{xz}}{\partial z} + \rho g \sin\theta, \tag{2}$$

$$\rho\left(\frac{\partial w}{\partial t} + u\frac{\partial w}{\partial x} + w\frac{\partial w}{\partial z}\right) = -\frac{\partial p}{\partial z} + \frac{\partial \tau_{xz}}{\partial x} + \frac{\partial \tau_{zz}}{\partial z} - \rho g \cos\theta, \tag{3}$$

where p is the pressure and u and w are the streamwise and cross-stream velocity components, respectively. The density is given by ρ, the gravitational acceleration is denoted by g while θ represents the angle of inclination of the plate. The components of the deviatoric stress tensor for a power-law fluid are given by $\tau_{xx} = 2\mu_n\eta\frac{\partial u}{\partial x}$, $\tau_{zx} = \tau_{xz} = \mu_n\eta\left(\frac{\partial u}{\partial z} + \frac{\partial w}{\partial x}\right)$ and $\tau_{zz} = 2\mu_n\eta\frac{\partial w}{\partial z}$, where

$$\eta = \left[2\left(\left(\frac{\partial u}{\partial x}\right)^2 + \left(\frac{\partial w}{\partial z}\right)^2\right) + \left(\frac{\partial u}{\partial z} + \frac{\partial w}{\partial x}\right)^2\right]^{\frac{(n-1)}{2}},$$

and μ_n and n are the consistency and power-law index, respectively. It is worth pointing out here that the classic Newtonian model is a particular case corresponding to $n = 1$, with the consistency being the Newtonian viscosity. For positive values of n less than unity the model depicts a shear-thinning flow, whereas $n > 1$ corresponds to a shear-thickening fluid.

In order to incorporate a temperature variation into the rheology of the fluid, we proceed as was done by Bernabeu et al.[26] and assume that the consistency of the fluid is a function of temperature. The usual assumption for the variation in viscosity is an exponential decrease with temperature which

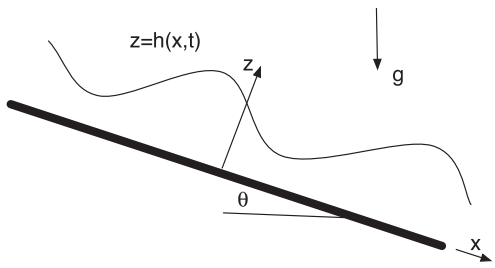

FIG. 1. Schematic representation of a thin film flowing down an inclined plane.

is referred to as the Arrhenius formulation. We linearize this relation with respect to temperature and assume that the consistency is given by

$$\mu_n = \hat{\mu}_n - \hat{\lambda}(T - T_\infty),$$

where T denotes the temperature, $\hat{\mu}_n$ is the value of the consistency at $T = T_\infty$ and $\hat{\lambda} > 0$ is a constant control parameter which measures the rate of change with respect to temperature.

By applying conservation of energy we obtain the following equation for the temperature of the fluid

$$\frac{\partial T}{\partial t} + u\frac{\partial T}{\partial x} + w\frac{\partial T}{\partial z} = \chi\left(\frac{\partial^2 T}{\partial x^2} + \frac{\partial^2 T}{\partial z^2}\right), \tag{4}$$

where χ is the thermal diffusivity.

We assume that the viscous stress exerted by the ambient gas on the surface is negligible. Therefore, the force exerted by the flow is balanced by the ambient pressure and the effect of surface tension. The normal component of the force balance is then given by

$$p = p_\infty + \frac{2\mu_n\eta}{1+\left(\frac{\partial h}{\partial x}\right)^2}\left[\left(\frac{\partial h}{\partial x}\right)^2\frac{\partial u}{\partial x} - \frac{\partial h}{\partial x}\left(\frac{\partial u}{\partial z} + \frac{\partial w}{\partial x}\right) + \frac{\partial w}{\partial z}\right] - \frac{\sigma\frac{\partial^2 h}{\partial x^2}}{\left(1+\left(\frac{\partial h}{\partial x}\right)^2\right)^{\frac{3}{2}}} \quad \text{at} \quad z = h(x,t), \tag{5}$$

and the tangential component can be expressed as

$$\left[\frac{\partial \sigma}{\partial x} + \frac{\partial h}{\partial x}\left(\frac{\partial \sigma}{\partial z}\right)\right]\sqrt{1+\left(\frac{\partial h}{\partial x}\right)^2} = \mu_n\eta\left[\left(1-\left(\frac{\partial h}{\partial x}\right)^2\right)\left(\frac{\partial u}{\partial z} + \frac{\partial w}{\partial x}\right) + 2\frac{\partial h}{\partial x}\left(\frac{\partial w}{\partial z} - \frac{\partial u}{\partial x}\right)\right] \quad \text{at} \quad z = h(x,t), \tag{6}$$

where p_∞ denotes the ambient pressure and σ represents the surface tension. The left-hand side of the tangential force balance relation is due to the so-called Marangoni stress which results from variation in surface tension, and pulls fluid along the surface in the direction of increasing surface tension.

The surface tension is assumed to depend linearly on the temperature and is expressed as

$$\sigma = \sigma_\infty - \sigma_t(T - T_\infty), \tag{7}$$

where σ_∞ is the surface tension of the fluid at the reference value $T = T_\infty$. The parameter σ_t is defined as

$$\sigma_t = -\frac{\partial \sigma}{\partial T} > 0. \tag{8}$$

So surface tension decreases with temperature.

A kinematic condition for the free surface of the liquid layer can be derived from the assumption that evaporation is negligible and expressed as

$$w = \frac{\partial h}{\partial t} + \frac{\partial h}{\partial x}u \quad \text{at} \quad z = h(x,t). \tag{9}$$

The relation between the heat flux normal to the surface and the difference in the temperature of the liquid and the ambient gas is expressed through Newton's law of cooling which is given by

$$-\kappa\nabla T \cdot \widehat{n} = \alpha(T - T_\infty) \quad \text{at} \quad z = h(x,t), \tag{10}$$

where α is the heat transfer coefficient, κ is the thermal conductivity and $\widehat{n}$ is the outward unit vector to the surface.

At the bottom interface appropriate boundary conditions arise from the requirement of no slip and no penetration and can be written as

$$u = w = 0 \quad \text{at} \quad z = 0, \tag{11}$$

and since the substrate is maintained at temperature T_w, we have the condition

$$T = T_w \quad \text{at} \quad z = 0. \tag{12}$$

We nondimensionalize the governing equations by scaling with quantities corresponding to the steady isothermal Nusselt flow. For a prescribed flow rate Q, the Nusselt thickness is given by

$$H = \left(\frac{\hat{\mu}_n}{\rho g \sin\theta}\right)^{\frac{1}{2n+1}} Q^{\frac{n}{2n+1}} \left(\frac{2n+1}{n}\right)^{\frac{n}{2n+1}}. \tag{13}$$

Now, we expect the flow to be destabilized by the amplification of perturbations much longer than the characteristic depth of the fluid layer. We will obtain approximate solutions based on this expectation. In order to be able to identify which terms in the governing equations are negligible, we use a different length scale in the streamwise direction and denote the ratio of H to this scale by δ. To scale the equations we introduce the following transformation

$$\begin{gathered}(x,z) = H\left(\frac{x^*}{\delta}, z^*\right),\ h = Hh^*,\ (u,w) = U(u^*, \delta w^*),\ t = \frac{H}{U\delta}t^*,\\ p - p_\infty = \rho\, U^2 p^*,\ T = T_\infty + \Delta T\, T^*,\end{gathered} \tag{14}$$

where $U = Q/H$ and $\Delta T = T_w - T_\infty$. Applying this scaling and removing the asterisk for notational convenience, the conservation equations (1)–(4) become

$$\frac{\partial u}{\partial x} + \frac{\partial w}{\partial z} = 0, \tag{15}$$

$$Re\,\delta\frac{Du}{Dt} = -Re\delta\frac{\partial p}{\partial x} + 2\delta^2\frac{\partial}{\partial x}\left[(1-\lambda T)\eta\frac{\partial u}{\partial x}\right] + \frac{\partial}{\partial z}\left[(1-\lambda T)\eta\left(\frac{\partial u}{\partial z} + \delta^2\frac{\partial w}{\partial x}\right)\right] + \left(\frac{2n+1}{n}\right)^n, \tag{16}$$

$$Re\,\delta^2\frac{Dw}{Dt} = -Re\frac{\partial p}{\partial z} + 2\delta\frac{\partial}{\partial z}\left[(1-\lambda T)\eta\frac{\partial w}{\partial z}\right] + \delta\frac{\partial}{\partial x}\left[(1-\lambda T)\eta\left(\frac{\partial u}{\partial z} + \delta^2\frac{\partial w}{\partial x}\right)\right] - \left(\frac{2n+1}{n}\right)^n \cot\theta, \tag{17}$$

$$\delta RePr\left(\frac{\partial T}{\partial t} + u\frac{\partial T}{\partial x} + w\frac{\partial T}{\partial z}\right) = \delta^2\frac{\partial^2 T}{\partial x^2} + \frac{\partial^2 T}{\partial z^2}, \tag{18}$$

where

$$\eta = \left[2\delta^2\left(\left(\frac{\partial u}{\partial x}\right)^2 + \left(\frac{\partial w}{\partial z}\right)^2\right) + \left(\frac{\partial u}{\partial z} + \delta^2\frac{\partial w}{\partial x}\right)^2\right]^{\frac{(n-1)}{2}},$$

the Reynolds number is defined as $Re = \frac{\rho}{\hat{\mu}_n} U^{2-n} H^n$, the Prandtl number is given by $Pr = \frac{\hat{\mu}_n}{\rho\chi}\left(\frac{U}{H}\right)^{n-1}$ and $\lambda = \frac{\hat{\lambda}\Delta T}{\hat{\mu}_n}$. Applying the scaling to the continuity of normal stress condition at the free surface yields

$$p = \frac{2\delta}{ReF^2}\eta(1-\lambda T)\left[\delta^2\left(\frac{\partial h}{\partial x}\right)^2\frac{\partial u}{\partial x} + \frac{\partial w}{\partial z} - \frac{\partial h}{\partial x}\left(\frac{\partial u}{\partial z} + \delta^2\frac{\partial w}{\partial x}\right)\right] - \frac{\delta^2}{F^3}\frac{\partial^2 h}{\partial x^2}(We - MT), \tag{19}$$

where

$$F = \left[1 + \delta^2\left(\frac{\partial h}{\partial x}\right)^2\right]^{\frac{1}{2}},$$

$We = \frac{\sigma_\infty}{\rho U^2 H}$ is the Weber number, which is proportional to the surface tension strength, and $M = \frac{\sigma_t \Delta T}{\rho U^2 H}$, which measures the variation in surface tension and is sometimes referred to as the film Marangoni number. The scaled continuity of tangential stress condition at the free surface, $z = h(x, t)$, can be written as

$$-\delta MF\left(\frac{\partial T}{\partial x} + \frac{\partial T}{\partial z}\frac{\partial h}{\partial x}\right) = \frac{\eta(1-\lambda T)}{Re}\left[\left(1 - \delta^2\left(\frac{\partial h}{\partial x}\right)^2\right)\left(\delta^2\frac{\partial w}{\partial x} + \frac{\partial u}{\partial z}\right) - 4\delta^2\frac{\partial h}{\partial x}\frac{\partial u}{\partial x}\right]. \tag{20}$$

Applying the scaling to the Newton's law of cooling yields

$$\frac{\partial T}{\partial z} - \delta^2 \frac{\partial h}{\partial x}\frac{\partial T}{\partial x} = -BFT \quad \text{at} \quad z = h(x,t), \tag{21}$$

where $B = \frac{\alpha H}{\kappa}$. The kinematic condition becomes

$$w = \frac{\partial h}{\partial t} + u\frac{\partial h}{\partial x} \quad \text{at} \quad z = h(x,t), \tag{22}$$

and the remaining boundary conditions at $z = 0$ are non-dimensionalized to give

$$u = 0, \quad w = 0, \quad T = 1 \quad \text{at} \quad z = 0. \tag{23}$$

Equations (15)–(23) represent the dimensionless form of the full equations governing the flow. We simplify these equations by discarding certain terms based on the assumed smallness of the ratio of cross-stream to streamwise length scales. To obtain the long-wave equations we let δ tend to zero and discard the $O(\delta^2)$ terms from equations (15)–(23), while assuming all the other parameters to be $O(1)$, with the exception of the Weber number, which is assumed large enough so that $\delta^3 We = O(1)$. This allows us to eliminate the pressure from the problem. Specifically, the z-momentum equation and the continuity of normal force condition, equations (17) and (19), reduce to

$$\frac{\partial p}{\partial z} = -\left(\frac{2n+1}{n}\right)^n \frac{\cot\theta}{Re}$$

and

$$p = -\delta^2 We \frac{\partial^2 h}{\partial x^2} \quad \text{at} \quad z = h(x,t),$$

which yields the following expression for the pressure

$$p = \left(\frac{2n+1}{n}\right)^n \frac{\cot\theta}{Re}(h - z) - \delta^2 We \frac{\partial^2 h}{\partial x^2}.$$

In obtaining these equations we also discarded the $O(\delta)$ terms since the pressure is multiplied by δ in the $x-$momentum equation.

Once the negligible terms have been identified and discarded, we rescale the equations with scale H for both x and z. This can be accomplished by simply setting $\delta = 1$ in the current formulation. We thus get the long-wave equations consisting of

$$\frac{\partial u}{\partial x} + \frac{\partial w}{\partial z} = 0, \tag{24}$$

$$Re\left(\frac{\partial u}{\partial t} + u\frac{\partial u}{\partial x} + w\frac{\partial u}{\partial z}\right) = \frac{\partial}{\partial z}\left[(1 - \lambda T)\left(\frac{\partial u}{\partial z}\right)^n\right] - \left(\frac{2n+1}{n}\right)^n \cot\theta \frac{\partial h}{\partial x} + ReWe\frac{\partial^3 h}{\partial x^3} + \left(\frac{2n+1}{n}\right)^n, \tag{25}$$

$$PrRe\left(\frac{\partial T}{\partial t} + u\frac{\partial T}{\partial x} + w\frac{\partial T}{\partial z}\right) = \frac{\partial^2 T}{\partial z^2}, \tag{26}$$

with the conditions

$$-MRe\left(\frac{\partial T}{\partial x} + \frac{\partial T}{\partial z}\frac{\partial h}{\partial x}\right) = (1 - \lambda T)\left(\frac{\partial u}{\partial z}\right)^n, \quad \text{at} \quad z = h(x,t), \tag{27}$$

$$\frac{\partial T}{\partial z} = -BT \quad \text{at} \quad z = h(x,t), \tag{28}$$

$$w = \frac{\partial h}{\partial t} + u\frac{\partial h}{\partial x} \quad \text{at} \quad z = h(x,t), \tag{29}$$

$$u = 0, \quad w = 0, \quad T = 1 \quad \text{at} \quad z = 0. \tag{30}$$

III. LINEAR STABILITY ANALYSIS

The problem represented by equations (24)–(30) governing a falling power-law fluid film along a heated inclined plate admits a simple solution corresponding to a steady flow, uniform in the streamwise direction. In order to determine this equilibrium solution we set derivatives with respect to x and t to zero and assign the uniform thickness of the liquid layer to be $h = 1$. Using the notation $w = w_s$, $u = u_s$ and $T = T_s$, we thus obtain the following equations for the equilibrium flow

$$\frac{dw_s}{dz} = 0,$$
$$Re\, w_s \frac{du_s}{dz} = \frac{d}{dz}\left[(1 - \lambda T_s)\left(\frac{du_s}{dz}\right)^n\right] + \left(\frac{2n+1}{n}\right)^n, \tag{31}$$
$$\frac{d^2T_s}{dz^2} = PrRe\, w_s \frac{dT_s}{dz},$$

with the conditions at $z = 1$ being

$$\frac{du_s}{dz} = 0,$$
$$-BT_s = \frac{dT_s}{dz},$$

and at $z = 0$

$$u_s(0) = 0, \quad w_s(0) = 0, \quad T_s(0) = 1.$$

These equations can easily be solved for T_s and w_s and we obtain

$$w_s(z) \equiv 0, \tag{32}$$

and

$$T_s(z) = 1 - \left(\frac{B}{B+1}\right)z. \tag{33}$$

In order to obtain a closed-form solution for $u_s(z)$ we must resort to an approximation. At this stage, for illustrative purposes we present a rough approximation obtained by integrating equation (31) and linearize with respect to λ, which yields

$$\frac{du_s}{dz} = \frac{2n+1}{n^2(B+1)}[n(B+1) + (1 + (1-z)B)\lambda](1-z)^{\frac{1}{n}}.$$

Integrating this and applying the boundary conditions we obtain

$$\begin{aligned} u_s = \frac{1}{(B+1)(1+n)n}\Big\{ & B(1-z)^{\frac{1+n}{n}}\lambda\, nz - B(1-z)^{\frac{1+n}{n}}\lambda\, n + B(1-z)^{\frac{1+n}{n}}\lambda\, z \\ & - 2\,B(1-z)^{\frac{1+n}{n}}n^2 - B(1-z)^{\frac{1+n}{n}}\lambda - B(1-z)^{\frac{1+n}{n}}n + B\lambda\, n + 2\,Bn^2 - 2\,(1-z)^{\frac{1+n}{n}}\lambda\, n \\ & - 2\,(1-z)^{\frac{1+n}{n}}n^2 + B\lambda + nB - (1-z)^{\frac{1+n}{n}}\lambda - (1-z)^{\frac{1+n}{n}}n + 2\,\lambda\, n + 2\,n^2 + \lambda + n\Big\}. \end{aligned} \tag{34}$$

To perform a linear stability analysis we consider the perturbed equilibrium solution given by

$$h = 1 + \zeta(x,t), \quad u = u_s(z) + \tilde{u}(x,z,t), \quad w = \tilde{w}(x,z,t), \quad T = T_s(z) + \tilde{T}(x,z,t),$$

where ζ, $\tilde{u}$, $\tilde{w}$ and $\tilde{T}$ are the added infinitesimal perturbations.

Introducing the perturbed solution into the governing equations (24)–(30), then linearizing with respect to the infinitesimal perturbation variables we obtain

$$\frac{\partial \tilde{u}}{\partial x} + \frac{\partial \tilde{w}}{\partial z} = 0, \tag{35}$$

$$Re\left(\frac{\partial \tilde{u}}{\partial t} + u_s\frac{\partial \tilde{u}}{\partial x} + \tilde{w}\frac{du_s}{dz}\right) = -\mathcal{N}\cot\theta\frac{\partial \zeta}{\partial x} + ReWe\frac{\partial^3\zeta}{\partial x^3} + \frac{df_1}{dz}\tilde{T} + f_1\frac{\partial \tilde{T}_z}{\partial z} + \frac{df_2}{dz}\frac{\partial \tilde{u}}{\partial z} + f_2\frac{\partial^2\tilde{u}}{\partial z^2}, \tag{36}$$

$$PrRe\left(\frac{\partial \tilde{T}}{\partial t} + u_s\frac{\partial \tilde{T}}{\partial x} + \tilde{w}\frac{dT_s}{dz}\right) = \frac{\partial^2\tilde{T}}{\partial z^2}, \tag{37}$$

where $f_1 = -\lambda\left(\frac{du_s}{dz}\right)^n, f_2 = (1-\lambda T_s)n\left(\frac{du_s}{dz}\right)^{n-1}$ and $\mathcal{N} = \left(2+\frac{1}{n}\right)^n$.

Transferring the boundary conditions at the free surface $z = 1+\zeta$ to $z = 1$ and linearizing yields the following conditions

$$-MRe\left[\frac{\partial \tilde{T}}{\partial x} + \frac{\partial \zeta}{\partial x}\frac{dT_s}{dz}\right] = (1-\lambda T_s)\left(\frac{du_s}{dz}\right)^{n-1} n\left(\frac{\partial \tilde{u}}{\partial z} + \zeta\frac{d^2u_s}{dz^2}\right) \quad \text{at} \quad z = 1, \tag{38}$$

$$-B\tilde{T} = \frac{\partial \tilde{T}}{\partial z} + B\frac{dT_s}{dz}\zeta \quad \text{at} \quad z = 1, \tag{39}$$

and

$$\tilde{w} = \frac{\partial \zeta}{\partial t} + u_s\frac{\partial \zeta}{\partial x} \quad \text{at} \quad z = 1. \tag{40}$$

At $z = 0$ the conditions are

$$\tilde{u} = 0, \quad \tilde{w} = 0, \quad \tilde{T} = 0. \tag{41}$$

We next employ normal modes into the linearized perturbation equations which are defined as

$$\left(\tilde{u}, \tilde{w}, \tilde{T}, \zeta\right) = \left(\hat{u}(z), \hat{w}(z), \hat{T}(z), \hat{\zeta}\right)e^{ik(x-ct)},$$

where $\hat{\zeta}$ is a constant, k represents the perturbation wavenumber which is a real positive number, c is a complex number whose real part is the phase speed of the perturbation, while the product of the imaginary part and k gives the growth rate. Then the linearized perturbation equations (35)–(41) can be written as

$$D\hat{w} + ik\hat{u} = 0, \tag{42}$$

$$ikRe(u_s - c)\hat{u} + ReDu_s\hat{w} = -ik\left(\mathcal{N}\cot\theta + Re\ We\ k^2\right)\hat{\zeta} + Df_1\hat{T} + f_1D\hat{T} + Df_2D\hat{u} + f_2D^2\hat{u}, \tag{43}$$

$$PrRe\left[ik(u_s - c)\hat{T} + DT_s\hat{w}\right] = D^2\hat{T}, \tag{44}$$

where D denotes the differentiation with respect to z operator. Applying the normal modes defined above to the interface conditions at $z = 1$ gives

$$-ikMRe\left(\hat{T} + DT_s\hat{\zeta}\right) = (1-\lambda T_s)(Du_s)^{n-1}n\left[D\hat{u} + \hat{\zeta}D^2u_s\right] \tag{45}$$

$$-B\hat{T} = D\hat{T} + BDT_s\hat{\zeta}, \tag{46}$$

$$\hat{w} = ik(u_s - c)\hat{\zeta}. \tag{47}$$

While the boundary conditions evaluated at $z = 0$ will take the following form

$$\hat{u}(0) = \hat{w}(0) = \hat{T}(0) = 0. \tag{48}$$

We introduce the stream function, ψ, to satisfy the perturbed continuity equation (42). The stream function is related to the velocity disturbances $\tilde{u}$, $\tilde{w}$ and is defined as

$$\tilde{u}(x,z,t) = \frac{\partial \psi}{\partial z}, \ \tilde{w}(x,z,t) = -\frac{\partial \psi}{\partial x}.$$

In terms of the normal modes, ψ can be written as

$$\psi = \Psi(z)e^{ik(x-ct)}.$$

Then $\hat{u}$ and $\hat{w}$ are expressed as

$$\hat{u}(z) = D\Psi, \ \hat{w}(z) = -ik\Psi.$$

Consequently, we have the following Orr-Sommerfeld type equations

$$\begin{aligned} &f_2\,D^3\Psi + Df_2\,D^2\Psi + ik(c-u_s)Re\,D\Psi + ik\,Re\,Du_s\,\Psi \\ &\quad + Df_1\,\hat{T} + f_1\,D\hat{T} - ik(\mathcal{N}\cot\beta + Re\,We\,k^2)\,\hat{\zeta} = 0, \end{aligned} \tag{49}$$

$$D^2\hat{T} + ik\,Pr\,Re[(c-u_s)\,\hat{T} + DT_s\Psi] = 0. \tag{50}$$

The boundary conditions at $z = 1$ are

$$-ik\,M\,Re\left(\hat{T} + \hat{\zeta}\,DT_s\right) = (1-\lambda T_s)(Du_s)^{n-1}\,n\left[D^2\Psi + \hat{\zeta}\,D^2u_s\right], \tag{51}$$

$$-B\hat{T} = D\hat{T} + B\,DT_s\,\hat{\zeta}, \tag{52}$$

and

$$\Psi + u_s\,\hat{\zeta} = c\,\hat{\zeta}. \tag{53}$$

While the conditions at $z = 0$ are

$$\hat{T} = \Psi = D\Psi = 0. \tag{54}$$

The equations (49)–(54) constitute an eigenvalue problem with c being the parameter that is to be assigned eigenvalues. For a given set of flow parameters (Re, Pr, B, M, λ, n, θ, We), solving the problem for c provides the growth rate of the perturbation with wavenumber k. A positive value of the imaginary part of c, $\Im(c)$, indicates that the perturbation amplitude grows in time, whereas if this quantity is negative then the perturbation is reduced. A set of flow parameters for which $\Im(c) = 0$ is referred to as the state of neutral stability for the perturbation with wavenumber k, and corresponds to the threshold between stability and instability for this perturbation. Regarding the stability of the flow, if all the perturbations are damped then the flow is stable, otherwise it is unstable.

The solution of the eigenvalue problem (49)–(54) can be obtained as usual by carrying out an asymptotic analysis as $k \to 0$ based on the expectation that small wavenumber perturbations are the most unstable. However, to obtain an analytical expression for the neutral stability state we must also implement asymptotic expansions as $\lambda \to 0$. To correctly accomplish this we must relate the magnitudes of the two small parameters. Proceeding as done in Ref. 8 we assume that λ approaches 0 like $k^{1/4}$. We will assume quantities that are $O(k^2)$ to be negligibly small, and thus we also discard the $O(\lambda^8)$ terms. The specific asymptotic expansions of the perturbations $\Psi, \hat{T}, \hat{\zeta}$ and the eigenvalue c can be expressed as

$$\begin{aligned}
\Psi &= \psi_0(z) + k\psi_1(z),\\
\hat{T} &= \hat{T}_0(z) + k\hat{T}_1(z),\\
\hat{\zeta} &= \hat{\zeta}_0 + k\hat{\zeta}_1,\\
c &= c_0 + kc_1,
\end{aligned}$$

where the coefficients of the powers of k are expanded in powers of λ with the appropriate number of terms. For example, in the expansion of Ψ we must have

$$\psi_0(z) = \sum_{j=0}^{7} \psi_{0j}(z)\lambda^j \quad \text{and} \quad \psi_1(z) = \sum_{j=0}^{3} \psi_{1j}(z)\lambda^j.$$

Substituting into the system of equations (49)–(54), we then have a hierarchy of problems at different orders of k. Without loss of generality we can normalize the eigenvalue problem and set $\hat{\zeta}_0 = 1$ and $\hat{\zeta}_1 = 0$. Collecting the k-independent terms, we obtain

$$D^2\hat{T}_0 = 0, \quad D\hat{T}_0(1) + B\hat{T}_0(1) + BDT_s(1) = 0, \quad \hat{T}_0(0) = 0, \tag{55}$$

$$D\Big[n(1-\lambda T_s)(Du_s)^{n-1}D^2\psi_0\Big] - D\Big[\lambda(Du_s)^n\hat{T}_0\Big] = 0, \tag{56}$$

$$n(1-\lambda T_s)(Du_s)^{n-1}D^2\psi_0 = -n(1-\lambda T_s)(Du_s)^{n-1}D^2u_s \quad \text{at} \quad z = 1, \tag{57}$$

$$D\psi_0(0) = \psi_0(0) = 0, \tag{58}$$

$$\psi_0 + u_s = c_0 \quad \text{at} \quad z = 1. \tag{59}$$

Focusing now on the k terms gives

$$D^2\hat{T}_1 + iPrRe\Big[(c_0 - u_s)\hat{T}_0 + DT_s\psi_0\Big] = 0, \quad D\hat{T}_1(1) + B\hat{T}_1(1) = 0 \quad \hat{T}_1(0) = 0, \tag{60}$$

$$D\Big[n(1-\lambda T_s)(Du_s)^{n-1}D^2\psi_1\Big] - D\Big(\lambda(Du_s)^n\hat{T}_1\Big) = iRe(u_s - c_0)D\psi_0 - iReDu_s\psi_0 + i\mathcal{N}\cot\theta, \tag{61}$$

$$n(1-\lambda T_s)(Du_s)^{n-1}D^2\psi_1 = \frac{iMReB}{(B+1)^2} \quad \text{at} \quad z = 1, \tag{62}$$

$$D\psi_1(0) = \psi_1(0) = 0, \tag{63}$$

$$c_1 = \psi_1(1). \tag{64}$$

The system of equations given by (55) can be solved exactly for $\hat{T}_0$ and the solution is

$$\hat{T}_0 = \frac{B^2}{(1+B)^2} z. \tag{65}$$

Equations (56)–(58) can then be solved for ψ_0, and then c_0 is given by (59). Integrating equation (56) from $z = 1$ to z, using the boundary condition (57) and the fact $Du_s(1) = 0$ we obtain

$$n(1 - \lambda T_s)(Du_s)^{n-1} D^2\psi_0 - \lambda (Du_s)^n \hat{T}_0 = \mathcal{N}. \tag{66}$$

In order to solve this equation we must now employ the asymptotic expansions with respect to λ as described above. However, before performing this calculation, we observe that the solution will be real, and the expression for c_0 given by (59) will consequently also be real. But then the neutral stability relation is given by $0 = \Im(c) = \Im(c_1)$, and from (64) we then have $\Im(\psi_1(1)) = 0$ describing the state of neutral stability. Since ψ_1 is the coefficient of k in the asymptotic expansion it only needs to be expanded to λ^3, so all the leading-order terms with respect to k only need to be expanded to λ^3. Therefore, in order to solve the problem for ψ_0 we introduce the expansions

$$u_s(z) = \sum_{j=0}^{3} u_{sj}(z)\lambda^j \quad \text{and} \quad \psi_0(z) = \sum_{j=0}^{3} \psi_{0j}(z)\lambda^j,$$

into the problem for the equilibrium velocity and into equations (66) and (58). This leads to a hierarchy of problems at the various orders of λ. All these problems were solved exactly using the Maple computer algebra software. The details are of little importance and are thus omitted here.

Substituting these solutions into (60) and expanding $\hat{T}_1$ as

$$\hat{T}_1(z) = \sum_{j=0}^{3} \hat{T}_{1j}(z)\lambda^j,$$

leads to separate problems for the coefficients which were again solved using Maple. Similarly, we then solve the problem given by (61)–(63) for ψ_1 in the form

$$\psi_1(z) = \sum_{j=0}^{3} \psi_{1j}(z)\lambda^j.$$

As pointed out above, neutral stability is given by $\psi_1(1) = 0$, which, if solved for Re gives the critical Reynolds number for the onset of instability of infinitely long perturbations. We have obtained an explicit formulation for the neutral stability relation, however it is too long to display here. As an illustration we present an approximation obtained by considering the linearized relation with respect to λ. In this case, a weakly non-Newtonian approximation for power-law index values near $n = 1$ is given by

$$Re_{crit} = \frac{R_1}{R_2},$$

where

$$\begin{aligned} R_1 = {} & 6\,(3\,n+2)(B+1)^2(5\,n+2)(5\,n+3)(5\,n+1)(n+1)^3 n^2 (4\,n+1)(3\,n+1)\cot\theta \\ & \times \left(2\,B\lambda\,n + 3\,Bn^2 + B\lambda + Bn + 3\,\lambda\,n + 3\,n^2 + \lambda + n\right)(4\,n+3), \end{aligned} \tag{67}$$

$$R_2 = C_1 + C_2\lambda$$

and

$$\begin{aligned} C_1 = {} & -5376\,(B+1)\Big(10080\,B^2\ln(3)n + 4200\,BM\ln(3)n - 10080\,B^2\ln(3) - 92844\,B^2 n \\ & - 4200\,BM\ln(3) - 44705\,nBM + 20160\,B\ln(3)n + 82764\,B^2 + 40505\,BM - 20160\,\ln(3)B \\ & - 185688\,Bn + 10080\,n\ln(3) + 165528\,B - 10080\,\ln(3) - 92844\,n + 82764\Big), \end{aligned} \tag{68}$$

$$
\begin{aligned}
C_2 = &-1172247552 + 1334817792\,n - 3105636288\,B - 892433136\,B^3 - 2825821872\,B^2 \\
&+ 15052800\,B^2M\ln(3) + 15775032\,B^3Pr\,n + 24685848\,B^2Pr\,n - 51460992\,BPr\,n \\
&+ 142661120\,B^2Mn - 124326720\,B^3\ln(3)n - 127608320\,B^2M + 1016759856\,B^3n \\
&- 14222712\,B^3Pr - 22407768\,B^2Pr + 45977472\,BPr + 124326720\,B^3\ln(3) + 162570240\,\ln(3) \\
&+ 395115840\,B^2\ln(3) + 3220937712\,B^2n - 195175680\,BM + 433359360\,\ln(3)B \\
&- 162570240\,n\ln(3) - 15052800\,B^2M\ln(3)n - 22579200\,BM\ln(3)n + 22579200\,BM\ln(3) \\
&- 395115840\,B^2\ln(3)n + 217754880\,nBM - 433359360\,B\ln(3)n + 3538995648\,Bn. \qquad (69)
\end{aligned}
$$

We also present exact formulations of the neutral stability relation for certain particular cases. First of all, in the Newtonian case we obtain

$$Re_{crit} = \frac{D_1}{D_2},$$

where

$$D_1 = 1680(B+1)^2\cot\theta\,(3\,B\lambda + 4\,B + 4\,\lambda + 4),$$

and

$$
\begin{aligned}
D_2 = &(8064 + (231\,Pr + 18501)\lambda)B^3 + ((2240\,M + 339\,Pr + 58797)\lambda + 3360\,M + 24192)B^2 \\
&+ ((3360\,M - 816\,Pr + 64488)\lambda + 3360\,M + 24192)B + 24192\,\lambda + 8064.
\end{aligned}
$$

If we set $\lambda = 0$ in this result we arrive at

$$Re_{crit} = \frac{10\cot\theta(1+B)^2}{12(1+B)^2 + 5MB},$$

which coincides with the result obtained by D'Alessio et al.[27] for the case with constant viscosity. Finally, in the general power-law case under isothermal conditions we have

$$Re_{crit} = \frac{1}{2}\left(\frac{n}{2n+1}\right)^{2-n}(3n+2)\cot\theta\,,$$

which agrees with the formula reported by Fernandez-Nieto et al.[20]

Finally, we point out that the Weber number does not figure in the neutral stability of the flow. This is because the strength of surface tension does not affect very long surface perturbations. It is rather the variation in surface tension, gauged by the parameter M, that plays an important role in the Marangoni instability.

In order to effectively present our results, we first remind the reader of the basic physical mechanisms related to the instability of the flow.[28] Non-isothermal inclined film flow is subject to two types of long-wave instabilities: the H mode and the S mode. The H mode refers to the amplification of surface waves due to inertia, and is the only instability mechanism in an isothermal flow. The fluid ahead of a crest on a propagating wave must accelerate when the crest passes over it in order to obtain the faster velocity profile associated with the expanded cross section of the flow. However, fluid inertia resists this adjustment and essentially effectuates a deceleration which causes fluid to accumulate under the crest thus amplifying the amplitude of the wave. At the troughs, inertia accelerates the flow thus pulling fluid away which lowers the troughs which also acts to amplify the wave. Since sufficient inertia is required to destabilize the H mode, there is a critical Reynolds number such that the H mode is unstable if this value is exceeded.

If the liquid layer is also heated from below, then a temperature variation is induced along the surface if it is wavy due to differences in distance from the heated bottom. The crests of waves are colder, while the troughs are warmer. As such, surface tension is stronger at the crests and weaker at the troughs generating Marangoni stresses which pull fluid away from the troughs toward the crests thus amplifying the waves. So, thermocapillarity enhances the H mode and lowers the critical Reynolds number for instability.

Now the S mode refers to the instability that is due entirely to the Marangoni effect when the surface is flat (wavy perturbations being effectively damped due to low levels of inertia). In this

case thermocapillarity is generated by perturbations in surface temperature as opposed to differential heating resulting from position relative to the heated bottom. Fluid motion along the surface caused by Marangoni stresses, if sufficiently strong, destabilizes the equilibrium flow. Resisting this action is inertia which works to preserve the equilibrium flow. So, the S mode is unstable only if the Reynolds number is sufficiently small. The critical value increases with the strength of the thermocapillarity.

The upshot then is that for weak enough thermocapillarity there are two critical Reynolds numbers: one for the S mode and a larger one for the H mode. For Reynolds numbers in the interval in between the equilibrium flow is stable while outside the interval it is unstable, due to the S mode for the smaller values and due to the H mode for the larger Reynolds numbers. As the level of thermocapillarity is increased, the interval of stable Reynolds numbers shrinks and eventually the two modes merge rendering the flow unstable for all Reynolds numbers.

In order to determine both critical Reynolds numbers, we must redefine some of our current control parameters. It turns out that B, M and We are implicitly dependent on the Reynolds number. To make this explicit we now express them as

$$B = \left[\csc\theta\left(\frac{2n+1}{n}\right)^n\right]^{\frac{2-n}{n+2}} Re^{\frac{n}{n+2}} Bi,$$

$$M = \left[\csc\theta\left(\frac{2n+1}{n}\right)^n\right]^{\frac{3n-2}{n+2}} Re^{-\frac{3n+2}{n+2}} Ma$$

and

$$We = \left[\left(\frac{2n+1}{n}\right)^n \csc\theta\right]^{\frac{3n-2}{n+2}} \frac{Ka}{Re^{\frac{3n+2}{n+2}}},$$

where

$$Bi = \frac{\alpha}{\kappa}\left(\frac{\mu_n}{\rho}\right)^{\frac{2}{n+2}} g^{\frac{n-2}{n+2}}, \quad \text{is the Biot number,}$$

$$Ma = \left(\frac{\rho}{\mu_n}\right)^{\frac{4}{n+2}} g^{\frac{2-3n}{n+2}} \sigma_t \Delta T, \quad \text{is the Marangoni number,}$$

and

$$Ka = \sigma\left(\frac{\rho^{2-n}}{g^{3n-2}\mu_n^4}\right)^{\frac{1}{n+2}}, \quad \text{is the Kapitza number.}$$

The Biot number is the scaled heat transfer coefficient of the free surface. The Kapitza number specifies the magnitude of surface tension, while the Marangoni number is proportional to its variation with temperature and measures the level of thermocapillarity for the system. Substituting these expressions for B and M into our asymptotic neutral stability relation results in a much more complicated formula that must be solved for Re numerically. We accomplished this by employing the Matlab subroutine fsolve.

In order to obtain results that are not restricted to small values of k and λ, we can solve the eigenvalue problem (49)–(54) numerically. We resorted to a collocation method based on polynomial interpolation with Chebyshev points.[29] In accordance with this approach, we introduced the expansions

$$\Psi = \sum_{j=0}^{N} w_j P_j(\xi), \quad \hat{T} = \sum_{j=0}^{N} v_j P_j(\xi),$$

where $\xi = 2z - 1$ and

$$P_j(\xi) = \frac{\prod_{\substack{n=0 \\ n\neq j}}^{N} (\xi - \xi_n)}{\prod_{\substack{n=0 \\ n\neq j}}^{N} (\xi_j - \xi_n)}, \; j = 0, 1, 2, \ldots, N,$$

with $\xi_l = -\cos\left(\frac{l\pi}{N}\right)$, $l = 0, 1, 2, \ldots, N$. This leads to an algebraic system of the form

$$\mathcal{A}y = c\mathcal{B}y,$$

where

$$y = [w_0\, w_1\, \cdots\, w_N\, v_0\, v_1\, \cdots\, v_N\, \hat{\eta}]^T,$$

and $\mathcal{A}$ and $\mathcal{B}$ are $(2N+3)\times(2N+3)$ matrices. The eigenvalues of this system were determined using the Matlab subroutine eig. From this set of eigenvalues, the single, physically relevant eigenvalue for the system (49)–(54) was selected by recalculating the eigenvalues of the algebraic system for a finer grid and identifying the value that persisted.

It turns out however, that this method fails to converge as more terms are added to the expansion when applied directly to the formulation of the problem given in (49)–(54). The cause is the fact that the non-Newtonian power-law model yields unbounded shear stress gradients for vanishing shear rates. To sidestep this issue we make an adjustment to the power-law model by replacing the long-wave approximation of the apparent viscosity by

$$\eta = \left[\epsilon + \left(\frac{\partial u}{\partial z}\right)^2\right]^{(n-1)/2},$$

where ϵ is the adjustment parameter for which we considered non-negative values, with $\epsilon = 0$ corresponding to the standard power-law model. Carrying out the linear stability analysis on the governing equations associated with the adjusted model results in the same eigenvalue problem as (49)–(54) with the exception that in equation (49) the coefficients f_1 and f_2 are given by

$$f_1 = -\lambda\left[\epsilon + \left(\frac{du_s}{dz}\right)^2\right]^{(n-1)/2}\frac{du_s}{dz}, \quad \text{and} \quad f_2 = (1-\lambda T_s)\left[\epsilon + \left(\frac{du_s}{dz}\right)^2\right]^{(n-3)/2}\left[\epsilon + n\left(\frac{du_s}{dz}\right)^2\right],$$

and the equilibrium velocity is obtained by numerically solving the equation

$$(1-\lambda T_s)\left[\epsilon + \left(\frac{du_s}{dz}\right)^2\right]^{(n-1)/2}\frac{du_s}{dz} = \mathcal{N}(1-z).$$

The collocation method functions properly in solving the adjusted eigenvalue problem, but only if ϵ is sufficiently large. However, as it is illustrated by the neutral stability curves displayed in Figure 2, we found that as ϵ is decreased there is an interval of values that are large enough for numerical convergence, and also yield results that are essentially independent of ϵ. We used a value in this range to generate the solutions used in our investigation.

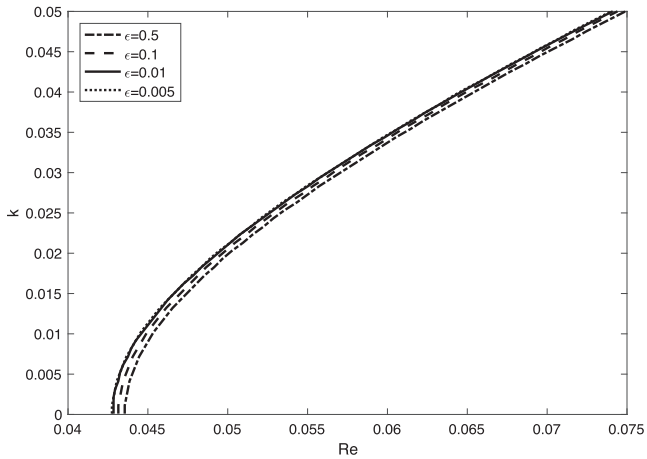

FIG. 2. Neutral stability curves corresponding to the H mode for different values of ϵ with $\cot\beta = 1$, $Pr = 7$, $Bi = 1$, $Ka = 100$, $n = 0.5$, $Ma = 1$, and $\lambda = 0.25$.

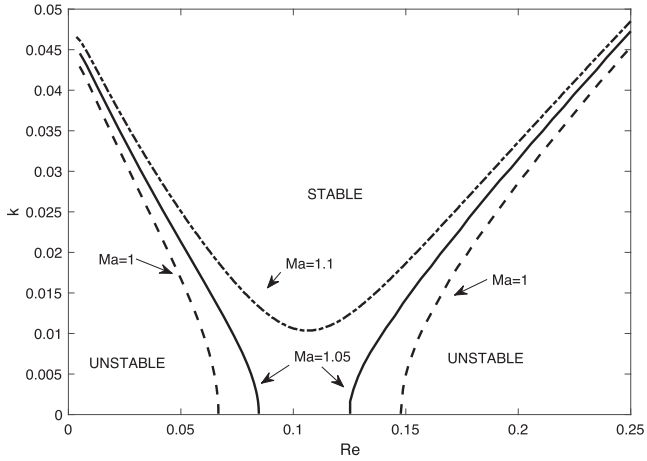

FIG. 3. Neutral stability curves for different values of Ma with $\cot\beta = 1$, $Pr = 7$, $Bi = 1$, $Ka = 100$, $n = 0.8$, and $\lambda = 0.25$.

In Figure 3 we present neutral stability curves in the $Re - k$ plane for different values of the Marangoni number. As it can be observed, for sufficiently small values of Ma the H and S modes correspond to two separate curves. In these cases for every perturbation there is a specific interval of Reynolds numbers for which the perturbation is damped. More specifically, these values of Re are sufficiently large to stabilize the S mode yet not large enough to trigger the H mode. The infinitely long perturbations have the smallest such interval and for these Reynold numbers the equilibrium flow is stable. The end points of the interval, given by the intercepts of the curves with the Re axis, thus give the critical Reynolds numbers for the onset of instability in the equilibrium flow.

In Figure 4 we compare these values with the results from the asymptotic analysis. We find good agreement for the critical Reynolds number for the S mode for a wide range of λ values, however, for the H mode the agreement is restricted to smaller values of this parameter.

In order to present the results from our investigation we plot the critical Reynolds numbers as a function of the Marangoni number. As it can be seen in Figure 5 for example, these curves consist of two branches: The upper branch which tracks the critical Reynolds number for the H mode and the lower branch corresponding to the S mode. The region inside the curve reveals the evolution of the interval of stable Reynolds numbers with Ma. Before we examine these results we point out that in all cases considered, like the one presented in Figure 3, we found the infinitely long perturbations

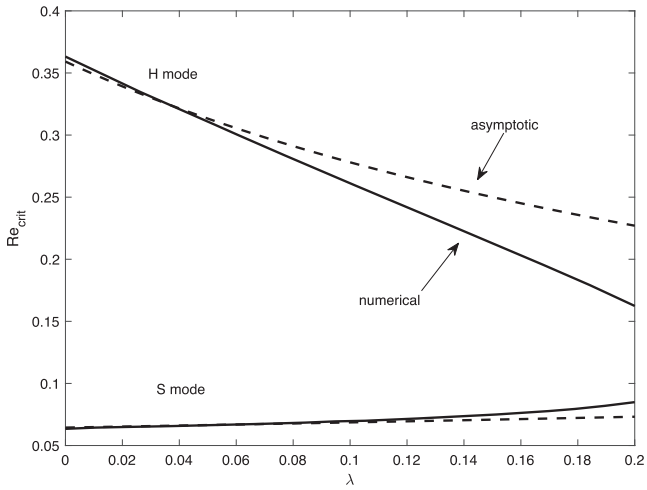

FIG. 4. Re_{crit} as a function of λ for $\cot\theta = 1$, $Pr = 7$, $Bi = 1$, $n = 0.8$ and $Ma = 1.1$.

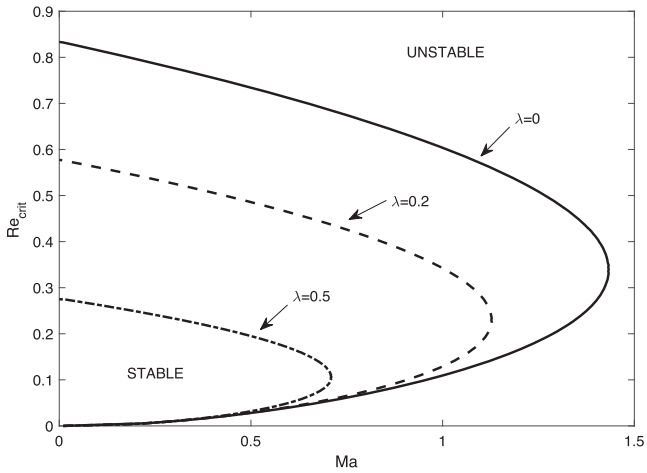

FIG. 5. Re_{crit} as a function of Ma for cot $\theta = 1$, $Pr = 7$, $Bi = 1$, $n = 1$.

to be the most unstable and are the ones that destabilize the equilibrium flow. As the magnitude of surface tension has little effect on the stability of these perturbations, the critical Reynolds number for the onset of instability is independent of the Kapitza number.

We begin by determining how the temperature dependence of the fluid rheology affects the stability of the flow. To accomplish this, in Figures 5 and 6 we plot the Re_{crit} versus Ma curves for different values of λ. We first consider the Newtonian case in Figure 5. Clearly, for a Newtonian fluid increasing λ results in a lower viscosity. Also, if we calculate the flow rate in the equilibrium flow we obtain

$$q_s = \int_0^1 u_s(z)dz = 1 + \frac{(3B+4)\lambda}{4B+4},$$

which increases with λ. Examining the results in Figure 5 reveals that Re_{crit} on the upper branch decreases with λ, indicating that the H mode is destabilized. This is most likely a consequence of a faster flow rate which boosts the destabilizing acceleration and deceleration phenomenon brought about by surface waves.

Looking now at the S mode in Figure 5 we see that there is no significant effect due to varying λ, with the exception of cases with greater thermocapillarity. In these cases increasing λ has a destabilizing effect. The culprit could possibly be the reduction in viscosity which allows for a stronger fluid motion along the surface generated by the Marangoni stresses.

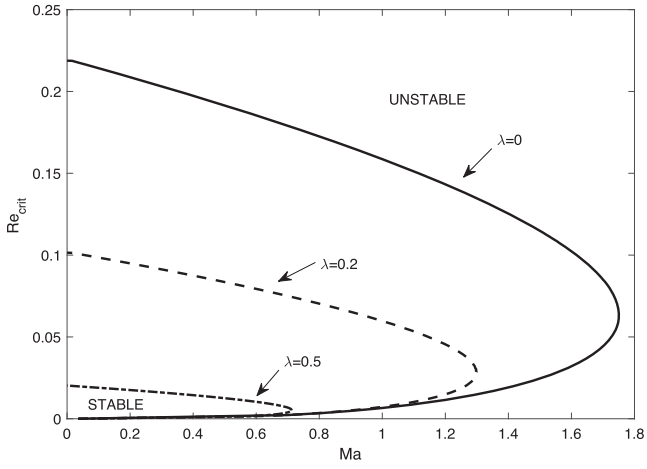

FIG. 6. Re_{crit} as a function of Ma for cot $\theta = 1$, $Pr = 7$, $Bi = 1$, $n = 0.5$.

In Figure 6 we consider the effect of λ on the stability of the flow for a non-Newtonian fluid which can be obtained from our model by setting the power-law index to $n \neq 1$. It is apparent from these results that a temperature dependent consistency has the same qualitative effect as for a Newtonian fluid. In the non-Newtonian case we do not have a "viscosity" in the Newtonian sense. We can instead think of an "apparent" viscosity defined as $\mu_{app} = \mu_n \left(\frac{\partial u}{\partial z}\right)^{n-1}$. For the equilibrium flow this is given by

$$\mu_{app} = \left(\frac{2n+1}{n}\right)^{n-1} (1-z)^{1-1/n} (1-\lambda T_s)^{1/n}, \quad 0 < z < 1,$$

which, like the Newtonian viscosity, is a decreasing function of λ. And the flow rate is given by

$$q_s = 1 + \frac{[(2B+3)n + B + 1]}{n(3n+1)(B+1)}\lambda,$$

which increases with λ for all the relevant values of n.

We next explore the effect of the non-Newtonian nature of the fluid on the stability of the flow. In Figure 7 we display the Re_{crit} as a function of Ma curves for different values of n. It can be seen that the critical Reynolds number for the S mode increases with n. Since the S mode is stabilized by inertia, and is thus unstable for subcritical Reynolds numbers, we can therefore say that the S mode becomes more unstable as n is increased. Re_{crit} for the H mode also increases, however this indicates a stabilizing effect, as stronger inertia is required to destabilize the flow. Now with respect to the non-Newtonian rheology of the fluid, we choose to consider that decreasing n with values less than unity renders the fluid more shear thinning, while if $n > 1$ the fluid is shear thickening, and increasing n strengthens the effect. We therefore conclude that shear thinning acts to stabilize the S mode and destabilize the H mode. Conversely, shear thickening is a destabilizing factor for the S mode, while it acts to stabilize the H mode.

Another interesting observation to be made from Figure 7 is that the lateral extent of the region of stability becomes longer as n is decreased or increased away from unity. This indicates that there are Marangoni numbers for which a Newtonian fluid is unstable for any Reynolds number, but a non-Newtonian fluid, with either a shear thinning or shear thickening behaviour, would be stable for a certain range of Reynolds numbers.

We next focus on the effect of the heat transfer across the surface between the liquid and the ambient gas which is measured by the Biot number. We begin by considering the limiting cases $Bi = 0$ and $Bi \to \infty$. If Bi is set to zero then Newton's law of cooling dictates that the heat flux across the surface is prescribed to be zero and consequently the equilibrium flow is isothermal (same temperature throughout). Therefore, even if the surface is wavy its temperature is uniform and so thermocapillarity does not contribute to the amplification of surface waves. At the other extreme we

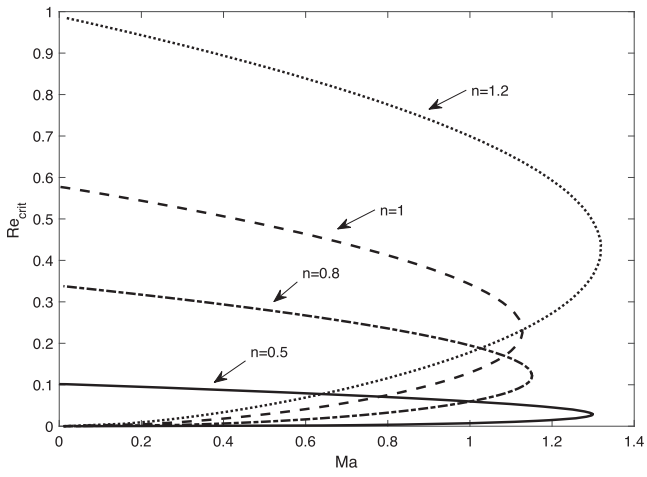

FIG. 7. Re_{crit} as a function of Ma for $\cot\theta = 1$, $Pr = 7$, $Bi = 1$, $\lambda = 0.2$.

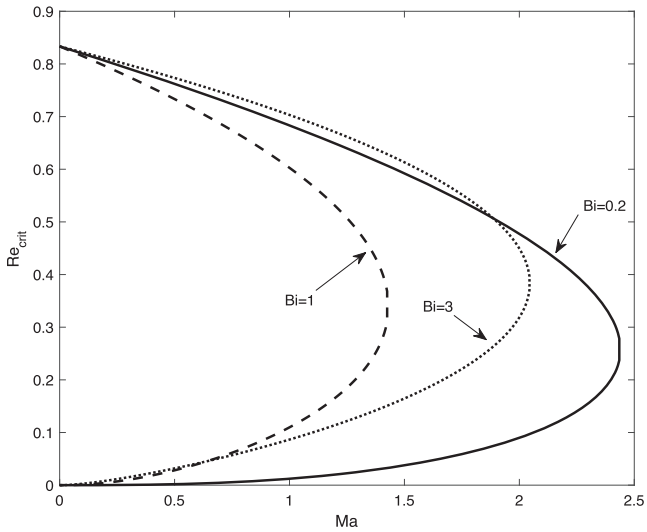

FIG. 8. Re_{crit} as a function of Ma for $\cot\theta = 1$, $Pr = 7$, $\lambda = 0$, $n = 1$.

have a similar situation. As $Bi \to \infty$ the condition at the surface approaches that of the ambient gas. In this case the surface temperature does not experience any variation in temperature and thus the Marangoni effect does not occur. Therefore, as we increase Bi from zero we expect thermocapillarity to strengthen and the flow to become more unstable. However, this trend must eventually reverse since for large values of Bi thermocapillarity becomes weaker.

In Figure 8 we consider the Newtonian case and show the critical Reynolds number curves for different values of Bi with $\lambda = 0$ (i.e. no temperature dependence of the consistency of the fluid). In accordance with the expectation described above, we see that for smaller values of Bi the region of stability contracts as this parameter is increased, but it begins to expand with Bi for sufficiently large values.

Now, if we introduce temperature variation in the viscosity we discover an interesting correlation. Specifically, we find that for sufficiently small Marangoni numbers the critical Reynolds number for the H mode actually increases with Bi. To illustrate this, in Figure 9 we plot Re_{crit} as a function of Bi. To explain this behaviour we point out that with $Bi = 0$ we have $T_s(z) \equiv 1$ (this being the largest possible temperature value), and so the viscosity is reduced by the maximum amount. Now, as explained above, lowering the viscosity destabilizes the flow. So, increasing Bi has a stabilizing

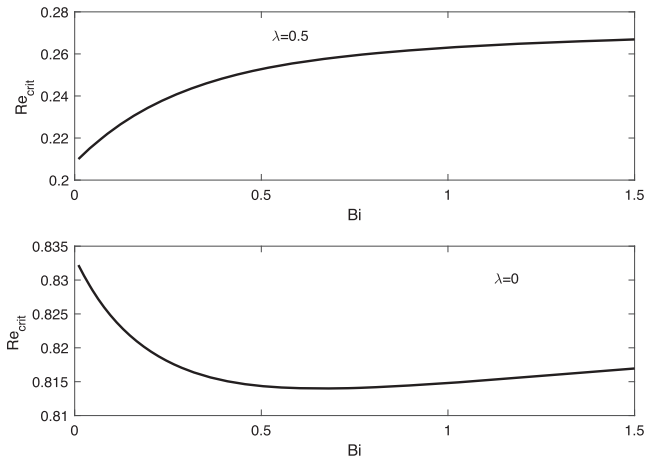

FIG. 9. Re_{crit} for the H mode as a function of Bi for $\cot\theta = 1$, $Pr = 7$, $Ma = 0.1$, $n = 1$.

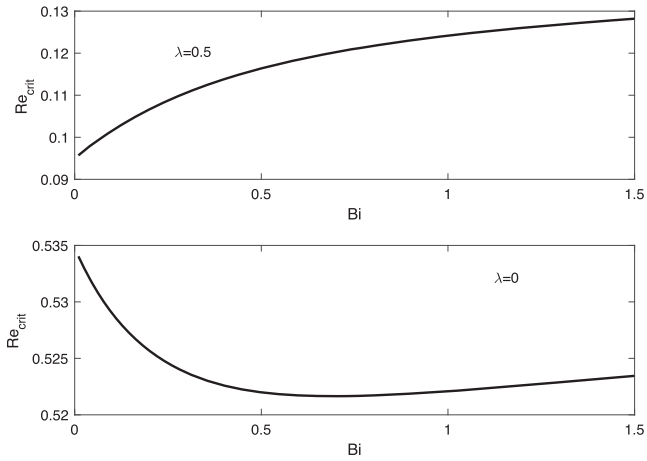

FIG. 10. Re_{crit} for the H mode as a function of Bi for $\cot\theta = 1$, $Pr = 7$, $Ma = 0.1$, $n = 0.8$.

effect because it relaxes the reduction in viscosity. Yes, it is true that increasing the Biot number from zero also unleashes destabilizing thermocapillarity, however if the surface tension is only weakly dependent on temperature differences (small Ma) the stabilizing effect of increasing the viscosity dominates the Marangoni instability. This phenomenon is also found for the non-Newtonian case, as it is illustrated in Figure 10, where we have set $n = 0.8$.

To conclude our analysis of the results we plotted the Re_{crit} as a function of Ma curves for different Prandtl numbers ranging from 0 to 20. We found these curves to be very close together and almost indistinguishable on the plot, and we do not display the figure here. But we conclude that varying the Prandtl number has little effect on the stability of the flow.

IV. NONLINEAR EFFECTS

Here we investigate the impact of nonlinear effects by implementing a first-order IBL model. This is achieved by integrating the governing equations across the fluid layer, and hence, eliminating the z dependence. We begin by retaining all terms up to first order in δ in equations (15)–(18) which yields the long-wave equations given by

$$\frac{\partial u}{\partial x} + \frac{\partial w}{\partial z} = 0, \tag{70}$$

$$Re\delta\left(\frac{\partial u}{\partial t} + u\frac{\partial u}{\partial x} + w\frac{\partial u}{\partial z}\right) = -Re\delta\frac{\partial p}{\partial x} + \frac{\partial}{\partial z}\left[(1-\lambda T)\left(\frac{\partial u}{\partial z}\right)^n\right] + \left(\frac{2n+1}{n}\right)^n, \tag{71}$$

$$0 = -Re\frac{\partial p}{\partial z} - \left(\frac{2n+1}{n}\right)^n \cot\theta, \tag{72}$$

$$\delta RePr\left(\frac{\partial T}{\partial t} + u\frac{\partial T}{\partial x} + w\frac{\partial T}{\partial z}\right) = \frac{\partial^2 T}{\partial z^2}. \tag{73}$$

We note that only the leading order terms in the z-momentum equation need to be kept since the pressure term in the x-momentum equation is already multiplied by δ.

Likewise we retain all terms up to first order in δ in the associated boundary conditions which in the absence of surface tension become

$$p = p_\infty, \tag{74}$$

$$-M\delta\left(\frac{\partial T}{\partial x} + \frac{\partial T}{\partial z}\frac{\partial h}{\partial x}\right) = \frac{(1-\lambda T)}{Re}\left(\frac{\partial u}{\partial z}\right)^n, \tag{75}$$

$$\frac{\partial T}{\partial z} = -BT, \tag{76}$$

$$w = \frac{\partial h}{\partial t} + u\frac{\partial h}{\partial x}, \tag{77}$$

along $z = h(x, t)$ and at the solid surface we have the usual no-slip, impermeability and fixed temperature conditions

$$u = 0, \quad w = 0, \quad T = 1 \quad \text{at} \quad z = 0. \tag{78}$$

Next, we introduce the flow rate, q, and the interfacial temperature, $\phi(x, t) = T(x, z = h, t)$, as our new flow variables with

$$q = \int_0^h u dz.$$

Integrating the continuity equation across the fluid layer and imposing the kinematic condition yields

$$\frac{\partial h}{\partial t} + \frac{\partial q}{\partial x} = 0. \tag{79}$$

Integrating the hydrostatic equation (72) subject to condition (74) and substituting the result into the momentum equation (71) and again integrating across the fluid layer we obtain

$$\frac{\partial q}{\partial t} + \frac{\partial}{\partial x}\left[\int_0^h u^2 dz + \left(\frac{2n+1}{n}\right)^n \frac{\cot\theta}{2Re} h^2\right] = \left(\frac{2n+1}{n}\right)^n \frac{h}{Re\delta} + \left[\frac{(1-\lambda T)}{Re\delta}\left(\frac{\partial u}{\partial z}\right)^n\right]_{z=h} - \left[\frac{(1-\lambda T)}{Re\delta}\left(\frac{\partial u}{\partial z}\right)^n\right]_{z=0}. \tag{80}$$

The term

$$\left[\frac{(1-\lambda T)}{Re\delta}\left(\frac{\partial u}{\partial z}\right)^n\right]_{z=h},$$

on the right-hand side of (80) can be determined using condition (75). However, to make further progress we need to evaluate the terms

$$\int_0^h u^2 dz \quad \text{and} \quad \left[\frac{(1-\lambda T)}{Re\delta}\left(\frac{\partial u}{\partial z}\right)^n\right]_{z=0}.$$

In order to do this we assume a velocity profile given by

$$u = \frac{q}{Q_0} b_0,$$

where

$$b_0(x, z, t) = \left(\frac{2n+1}{n+1}\right) A_0\left[h^{\frac{n+1}{n}} - (h-z)^{\frac{n+1}{n}}\right] + A_1\left[h^{\frac{2n+1}{n}} - (h-z)^{\frac{2n+1}{n}}\right] + \left(\frac{2n+1}{3n+1}\right) A_2\left[h^{\frac{3n+1}{n}} - (h-z)^{\frac{3n+1}{n}}\right],$$

$$A_0 = \frac{n^2(1+Bh)^2 + \lambda n(1+Bh) + (n+1)\lambda^2}{n^2(1+Bh)^2}, \; A_1 = \frac{\lambda B[n(1+Bh) + 2(n+1)\lambda]}{n^2(1+Bh)^2},$$

$$A_2 = \frac{(n+1)\lambda^2 B^2}{n^2(1+Bh)^2}, \; Q_0(x, t) = \int_0^h b_0 dz.$$

Thus, equation (80) becomes

$$\frac{\partial q}{\partial t} + \frac{\partial}{\partial x}\left[\int_0^h u^2 dz + M\phi + \left(\frac{2n+1}{n}\right)^n \frac{\cot\theta}{2Re} h^2\right] = \left(\frac{2n+1}{n}\right)^n \frac{h}{Re\delta}\left[1 - \left(1 + \frac{(n+1)\lambda^2}{2n}\right)\frac{q^n}{Q_0^n}\right], \tag{81}$$

where to leading order in λ we obtain

$$\int_0^h u^2 dz = \frac{2n^2 q^2 (1+Bh)^2 h^{\frac{3n+2}{n}}}{(2n+1)(3n+2)Q_0^2}, \; Q_0 = \frac{n(1+Bh)h^{\frac{2n+1}{n}}}{(2n+1)}.$$

The assumed u profile represents a second-order extension of the velocity profile given by equation (34) over the interval $0 \le z \le h$. An underlying assumption being made is that λ approaches 0 like $\sqrt{\delta}$. In addition, we also assume a linear temperature profile given by

$$T = 1 + \frac{(\phi - 1)}{h} z,$$

which follows directly from equation (33). To validate the assumed velocity profile we note that for selected values of n (such as $n = 1/2, 1, 2$) exact expressions for the uniform steady-state velocity can be obtained. These have been found to be

$$u_s = \alpha_0 \left[\frac{h(h + 2\alpha_1)}{\alpha_1 (h + \alpha_1)} + \frac{(z + \alpha_1)}{(h + \alpha_1)} - \frac{(h + \alpha_1)}{(z + \alpha_1)} + 2 \ln\left(\frac{\alpha_1}{z + \alpha_1} \right) \right] \text{ for } n = \frac{1}{2},$$

$$u_s = \alpha_0 \left[\frac{\alpha_1}{(h + \alpha_1)} - \frac{(z + \alpha_1)}{(h + \alpha_1)} + \ln\left(\frac{z + \alpha_1}{\alpha_1} \right) \right] \text{ for } n = 1,$$

$$u_s = \alpha_0 \left[\frac{\sqrt{(h - z)(z + \alpha_1)}}{h + \alpha_1} - \frac{\sqrt{\alpha_1 h}}{(h + \alpha_1)} + \arctan\left(\sqrt{\frac{h}{\alpha_1}} \right) - \arctan\left(\sqrt{\frac{h - z}{z + \alpha_1}} \right) \right] \text{ for } n = 2,$$

where

$$\alpha_0 = \frac{(2n + 1)(h + \alpha_1)}{n} \left(\frac{1 + Bh}{\lambda B} \right)^{\frac{1}{n}}, \; \alpha_1 = \frac{(1 - \lambda)(1 + Bh)}{\lambda B}.$$

Contrasted in Figure 11 is a comparison between b_0 and u_s for the parameter values $n = 1/2$, $\lambda = 0.1$, $h = 1$ and $B = 1$. We see that the agreement is very good. Although not presented, the agreement for $n = 1$ and $n = 2$ was found to be much better.

Applying the same approach to the energy equation we obtain

$$h \frac{\partial \phi}{\partial t} - \frac{1}{(4n + 1)(3n + 1)^2 (1 + Bh)} \left[n(\phi - 1) F_1 \frac{\partial q}{\partial x} + q F_2 \frac{\partial \phi}{\partial x} - \frac{n(2n + 1)\lambda B(\phi - 1) q}{(1 + Bh)} \frac{\partial h}{\partial x} \right]$$
$$= -\frac{2}{PrRe\delta h} [(1 + Bh)\phi - 1], \tag{82}$$

where

$$F_1 = (2n + 1)\lambda Bh - (3n + 1)(4n + 1)(1 + Bh), \; F_2 = n(2n + 1)\lambda Bh - (3n + 1)(4n + 1)^2 (1 + Bh).$$

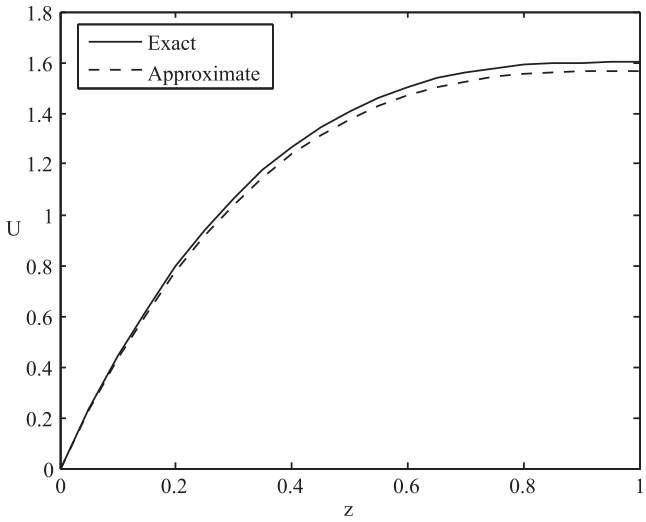

FIG. 11. Comparison between the assumed and exact velocity profiles for $n = 1/2$, $\lambda = 0.1$, $h = 1$, $B = 1$.

Thus, our first-order IBL model consists of equations (79), (81) and (82). As a check, if we perform a linear stability analysis on the system (79), (81), (82) with $\lambda = 0$ and $n = 1$ the following expression for Re_{crit} can be obtained

$$Re_{crit}^{IBL} = \frac{3\cot\theta(1+B)^2}{3(1+B)^2 + MB},$$

compared to

$$Re_{crit}^{full} = \frac{10\cot\theta(1+B)^2}{12(1+B)^2 + 5MB},$$

derived earlier. The ratio $Re_{crit}^{IBL}/Re_{crit}^{full}$ can be written as

$$\frac{Re_{crit}^{IBL}}{Re_{crit}^{full}} = 1.2\left[\frac{3(1+B)^2 + 1.25MB}{3(1+B)^2 + MB}\right],$$

and indicates the agreement in Re_{crit} between the IBL model and the full equations. Further, if $M = B = 0$ we get

$$Re_{crit}^{IBL} = \cot\theta,$$

which is in full agreement with the result predicted using the Shkadov IBL model[30] and the ratio $Re_{crit}^{IBL}/Re_{crit}^{full} = 1.2$. As a final check if we set $\lambda = M = B = 0$ then we obtain

$$Re_{crit}^{IBL} = \frac{n^{2-n}\cot\theta}{(2n+1)^{1-n}},$$

which recovers the expression obtained by Ng and Mei.[11] The agreement in Re_{crit} values for the H mode between the linearized full equations and nonlinear simulations resulting from the IBL model is illustrated in Figure 12 for the case $n = 0.8$, $\lambda = 0.1$, $B = 1$, $\cot\theta = 1$, $\delta = 0.1$ and $Pr = 7$ over the range $0 \le M \le 10$. The numerical solution procedure is outlined below. The agreement is reasonable and to be expected from a first-order IBL model. We see that the IBL model consistently predicts larger Re_{crit} values than those computed by the full equations and the difference between the two predictions seems to increase with M.

To obtain numerical solutions to the IBL equations we first introduce $\Phi = h(\phi - 1)$. From the relation $(T-1)h = (\phi - 1)z$ it follows that the variable Φ is related to T through

$$\int_0^h (T-1)dz = \frac{\Phi}{2},$$

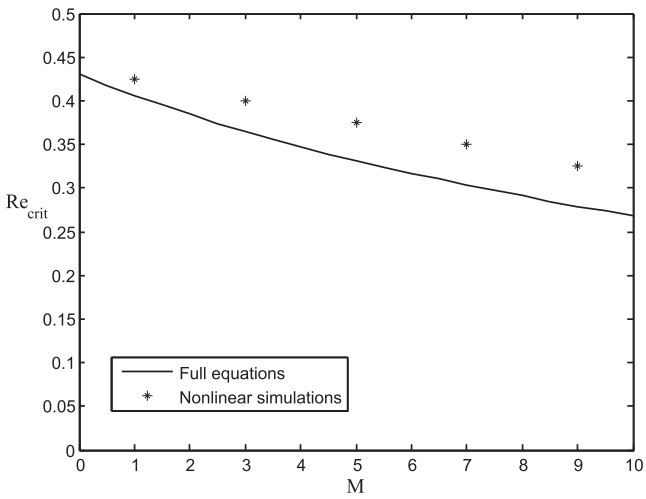

FIG. 12. Comparison in Re_{crit}.

and thus, Φ is proportional to the lineal heat content stored in the fluid layer. Equation (82) then becomes

$$\frac{\partial \Phi}{\partial t} + \frac{\partial}{\partial x}\left[\left(\frac{4n+1}{3n+1}\right)\frac{q\Phi}{h}\right] = \frac{n(2n+1)\lambda B}{(4n+1)(3n+1)^2(1+Bh)}\left[q\frac{\partial \Phi}{\partial x} + \Phi\frac{\partial q}{\partial x} - \frac{Bq\Phi}{(1+Bh)}\frac{\partial h}{\partial x}\right] - \frac{2}{PrRe\delta}\left[B + \frac{(1+Bh)\Phi}{h^2}\right]. \tag{83}$$

To numerically solve the system of equations (79), (81) and (83) we implement the fractional-step splitting technique,[31] that is, we first solve

$$\frac{\partial h}{\partial t} + \frac{\partial q}{\partial x} = 0,$$

$$\frac{\partial q}{\partial t} + \frac{\partial}{\partial x}\left[\int_0^h u^2 dz + \frac{M\Phi}{h} + \left(\frac{2n+1}{n}\right)^n \frac{\cot\theta}{2Re}h^2\right] = 0,$$

$$\frac{\partial \Phi}{\partial t} + \frac{\partial}{\partial x}\left[\left(\frac{4n+1}{3n+1}\right)\frac{q\Phi}{h}\right] = 0,$$

over a time step Δt, and then solve

$$\frac{\partial q}{\partial t} = \left(\frac{2n+1}{n}\right)^n \frac{h}{Re\delta}\left[1 - \left(1 + \frac{(n+1)\lambda^2}{2n}\right)\frac{q^n}{Q_0^n}\right],$$

$$\frac{\partial \Phi}{\partial t} = \frac{n(2n+1)\lambda B}{(4n+1)(3n+1)^2(1+Bh)}\left[q\frac{\partial \Phi}{\partial x} + \Phi\frac{\partial q}{\partial x} - \frac{Bq\Phi}{(1+Bh)}\frac{\partial h}{\partial x}\right] - \frac{2}{PrRe\delta}\left[B + \frac{(1+Bh)\Phi}{h^2}\right],$$

using the solution obtained from the first step as an initial condition for the second step. The second step then returns the solution for q and Φ at the new time $t + \Delta t$.

The first step involves solving a nonlinear system of hyperbolic conservation laws which, when expressed in vector form, can be written compactly as

$$\frac{\partial \mathbf{U}}{\partial \tau} + \frac{\partial \mathbf{F}(\mathbf{U})}{\partial X} = \mathbf{0},$$

where

$$\mathbf{U} = \begin{bmatrix} h \\ q \\ \Phi \end{bmatrix}, \quad \mathbf{F}(\mathbf{U}) = \begin{bmatrix} q \\ \int_0^h u^2 dz + \frac{M\Phi}{h} + \left(\frac{2n+1}{n}\right)^n \frac{\cot\theta}{2Re}h^2 \\ \left(\frac{4n+1}{3n+1}\right)\frac{q\Phi}{h} \end{bmatrix}.$$

While there are several schemes available to solve such a system, because of the complicated eigen-structure of the above system eigen-based methods will not be practical. Instead, MacCormack's method[31] was adopted due to its relative simplicity. This is a conservative second-order accurate finite difference scheme which correctly captures discontinuities and converges to the physical weak solution of the problem via the explicit predictor-corrector scheme

$$\mathbf{U}_j^* = \mathbf{U}_j^n - \frac{\Delta t}{\Delta x}\left[\mathbf{F}(\mathbf{U}_{j+1}^n) - \mathbf{F}(\mathbf{U}_j^n)\right],$$

$$\mathbf{U}_j^{n+1} = \frac{1}{2}\left(\mathbf{U}_j^n + \mathbf{U}_j^*\right) - \frac{\Delta t}{2\Delta x}\left[\mathbf{F}(\mathbf{U}_j^*) - \mathbf{F}(\mathbf{U}_{j-1}^*)\right],$$

where the notation $\mathbf{U}_j^n \equiv \mathbf{U}(x_j, t_n)$ is utilized with Δx denoting the uniform grid spacing and Δt is the time step. Since λ is typically a small parameter and h remains constant during the second step, the second step was solved by treating it as a coupled system of nonlinear ordinary differential equations which was solved iteratively using periodicity conditions at the left and right ends and using the output from the first step as an initial condition.

The evolution of the unsteady flow was computed by imposing a small perturbation on the constant steady-state solutions q_s, h_s and Φ_s where

$$h_s = 1,\ q_s = 1 + \frac{\lambda}{n(1+B)}\left[1 + \frac{(2n+1)B}{(3n+1)}\right],\ \Phi_s = -\frac{B}{(1+B)}.$$

By monitoring the growth of the disturbances as the perturbed solutions were marched in time we were able to determine the stability of the flow. We carried out a simulation using the parameter values $n = 0.8$, $\cot\theta = 1$, $M = 5$, $B = 1$, $Pr = 7$, $\delta = 0.1$, $\lambda = 0.1$ and $Re = 0.4$ which corresponds to an unstable H mode configuration. Computations were carried out on domains of lengths $L = 2$, 5 and 10 and the perturbation wavelength was set to be the domain length. The grid spacing and time step were taken to be $\Delta x = 0.01$ and $\Delta t = 0.001$. As a numerical check we computed the mass of the fluid layer at each time step and verified that mass was conserved to a high precision. Shown in Figure 13 is the time evolution of the fluid thickness, h, on a domain having a length $L = 2$. The diagram illustrates the growth and formation of a permanent series of two large amplitude waves as a result of the instability. Although not presented here, the flow rate, q, produces a similar plot but with different amplitudes. Because viscous terms are absent in our first-order IBL model the waves appear as sharp spikes. A higher-order model including viscous terms would yield shorter but wider waves as a result of the smearing effect brought on by viscosity. The only difference that resulted when a larger domain was used is in the number of waves appearing over the domain. As the domain length was increased so did the number of permanent waves. For example, with $L = 10$ a permanent series of four large amplitude waves emerged, while with $L = 5$ three waves were generated, and as noted above, only two waves were produced when $L = 2$. To ensure that Re_{crit} is independent of the domain length the nonlinear simulations shown in Figure 12 were carried out over a large domain length since the instability is triggered by perturbations having long wavelengths. We found from our numerical experiments that using $L = 10$ was sufficient, in that, the results obtained using $L = 10$ were identical to those using $L = 20$. Plotted in Figure 14 is a snap shot of the fluid thickness, h, and the surface temperature, ϕ, for the configuration shown in Figure 13 at $t = 10$. As already mentioned the variations in h align with the peaks in q; however, the surface temperature is out of phase with the fluid thickness, that is, the surface temperature is largest when h is smallest. This is because the steady-state temperature given by

$$T_s = 1 - \frac{B}{1+B}z,$$

decreases linearly with z. Thus, as h increases the surface temperature decreases.

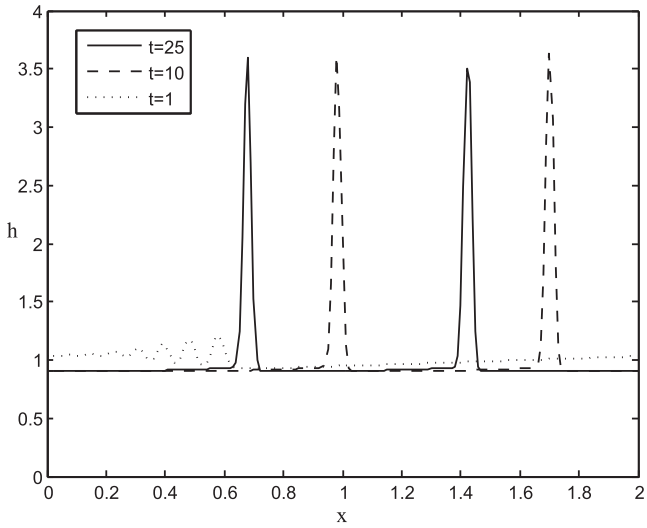

FIG. 13. Time evolution of the fluid thickness.

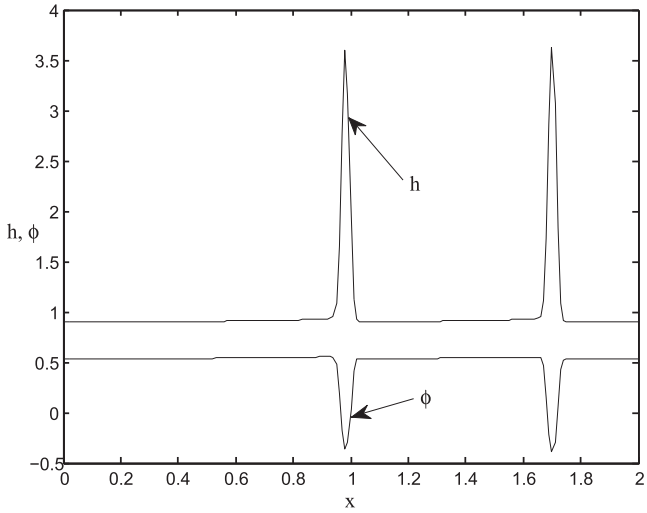

FIG. 14. The fluid thickness and surface temperature at $t = 10$.

V. CONCLUSIONS

In this investigation we derived a mathematical model for the flow of a liquid film down a heated incline. The rheology of the fluid is described by a power-law relation which includes the classic Newtonian fluid, but also allows for non-Newtonian behaviour. The model also accounts for variation with temperature in the properties of the fluid by implementing a temperature dependent formulation for the rheological relation. In addition, the model incorporates the realistic Newton's law of cooling at the surface of the liquid layer, which allows it to capture the enhancement to inertial instability provided by thermocapillarity.

We carried out a linear stability analysis to determine the critical conditions for the onset of long-wave instability in the steady flow uniform in the streamwise direction. We accounted for both relevant types of instability. One that is entirely due to thermocapillarity and is associated with slower flows (S mode), and the one that occurs in more rapid flows and consists of the amplification of surface waves due to inertial effects which is intensified by thermocapillarity (H mode). The S mode is stabilized by inertial effects (measured by the Reynolds number), while the opposite is the case for the H mode. Thermocapillarity raises the level of inertia necessary to stabilize the S mode and lowers the one sufficient to destabilize the H mode. As thermocapillarity is increased the two thresholds eventually coincide, the two modes are said to "merge", and beyond this level of thermocapillarity the flow is unstable for all Reynolds numbers.

Our investigation has revealed that a non-Newtonian rheology has an important impact on the stability of the flow. More specifically, shear thinning has a destabilizing effect on the H mode, i.e. when the instability is cause by the amplification of surface waves due to inertial effects. At low levels of inertia when the onset of instability is due entirely to the Marangoni effect, i.e. the S mode, shear thinning plays a stabilizing role by lowering the level of inertia required to prevent the Marangoni stresses from generating flow along the surface. Shear thickening, on the other hand, has the directly opposite effect: it stabilizes the H mode and destabilizes the S mode. We have also discovered that there are levels of thermocapillarity strong enough to destabilize a Newtonian flow for any Reynolds number, but are insufficient to have the same impact on a non-Newtonian fluid, shear thinning or shear thickening. For these fluids one can construct stable uniform flows, with inertia being large enough to prevent the S mode, but not enough so to trigger the H mode.

Regarding the effect of temperature variation in the consistency of the fluid, we found that it destabilizes both modes. Another interesting conclusion pertains to the correlation with the effect of heat transfer from the liquid to the ambient gas. In the idealized case of a perfectly insulated free surface, its equilibrium temperature is uniform even if undulations are generated by perturbations. In this case the Marangoni effect is decoupled from the amplification of surface undulations related

to inertial effects. As heat is allowed to start flowing across the surface the contribution to the amplification of surface undulations made by thermocapillarity becomes more and more significant and the flow is destabilized. But if the rheological nature of the fluid is affected by temperature the destabilization effect is reversed; increasing the heat transfer from the liquid results in a temperature distribution for which the destabilizing inertial effects themselves are weakened.

Lastly, nonlinear effects were also investigated based on a first-order IBL model. The agreement between theory and numerical simulations was reasonable and to be expected for a first-order model. The simulations reveal the formation of a permanent series of large amplitude waves for unstable configurations.

ACKNOWLEDGMENTS

Financial support for this research was provided by the Natural Sciences and Engineering Research Council of Canada and the Faculty of Mathematics at the University of Waterloo.

[1] S. Kalliadasis, E. A. Demekhin, C. Ruyer-Quil, and M. G. Velarde, "Thermocapillary instability and wave formation on a film falling down a uniformly heated plane," J. Fluid Mech. **492**, 303–338 (2003).
[2] C. Ruyer-Quil, B. Scheid, S. Kalliadasis, M. Velarde, and R. Zeytounian, "Thermocapillary long waves in a liquid film flow. Part 1. Low-dimensional formulation," J. Fluid Mech. **538**, 199–222 (2005).
[3] B. Scheid, C. Ruyer-Quil, S. Kalliadasis, M. Velarde, and R. Zeytounian, "Thermocapillary long waves in a liquid film flow. Part 2. Linear stability and nonlinear waves," J. Fluid Mech. **538**, 223–244 (2005).
[4] P. Trevelyan, B. Scheid, C. Ruyer-Quil, and S. Kalliadasis, "Heated falling films," J. Fluid Mech. **592**, 295–334 (2007).
[5] A. Hudoba and S. Molokov, "Linear stability of buoyant convective flow in a vertical channel with internal heat sources and a transverse magnetic field," Phys. Fluids **28**, 114103 (2016).
[6] D. A. Goussis and R. E. Kelly, "Effects of viscosity on the stability of film flow down heated or cooled inclined surfaces: Long-wavelength analysis," Phys. Fluids **28**, 3207–3214 (1985).
[7] C.-C. Hwang and C.-I. Weng, "Non-linear stability analysis of film flow down a heated or cooled inclined plane with viscosity variation," Int. J. Heat Mass Transfer **31**, 1775–1784 (1988).
[8] J. P. Pascal, N. Gonputh, and S. J. D. D'Alessio, "Long-wave instability of flow with temperature dependent fluid properties down a heated incline," Int. J. Eng. Sci. **70**, 73–90 (2013).
[9] S. J. D. D'Alessio, C. J. M. P. Seth, and J. P. Pascal, "The effects of variable fluid properties on thin film stability," Phys. Fluids **26**, 122105 (2014).
[10] B. M. Bates, N. Andreini, and C. Ancey, "Basal entrainment by Newtonian gravity-driven flows," Phys. Fluids **28**, 053101 (2016).
[11] C. Ng and C. C. Mei, "Roll waves on a shallow layer of mud modelled as a power-law fluid," J. Fluid Mech. **263**, 151–183 (1994).
[12] C. C. Hwang, J. L. Chen, J. S. Wang, and J. S. Lin, "Linear stability of power-law liquid film flow down an inclined plane," J. Phys. D **27**, 2297–2301 (1994).
[13] B. S. Dandapat and A. Mukhopadhyay, "Waves on a film of power-law fluid flowing down an inclined plate at moderate Reynolds number," Fluid Dyn. Res. **29**, 199–220 (2001).
[14] G. M. Sisoev, B. S. Dandapat, K. S. Matveyev, and A. Mukhopadhyay, "Bifurcation analysis of the travelling waves on a falling power-law fluid film," J. Non-Newtonian Fluid Mech. **141**, 128–137 (2007).
[15] C. Heining and N. Aksel, "Effects of inertia and surface tension on a power-law fluid flowing down a wavy incline," Int. J. Multiphase Flow **36**, 847–857 (2010).
[16] C. Di Cristo, M. Iervolino, and A. Vacca, "A strategy for passive control of natural roll-waves in power-law fluids through inlet boundary conditions," J. Appl. Fluid Mech. **10**, 667–680 (2017).
[17] M. Iervolino, J. P. Pascal, and A. Vacca, "Instabilities of a power-law film over an inclined permeable plane: A two-sided model," J. Non-Newtonian Fluid Mech. **259**, 111–124 (2018).
[18] E. Ellaban, J. P. Pascal, and S. J. D. D'Alessio, "Instability of a binary liquid film flowing down a slippery heated plate," Phys. Fluids **29**, 092105 (2017).
[19] M. Amaouche, A. Djema, and L. Bourdache, "A modified Shkadov's model for thin film flow of a power law fluid over an inclined surface," C. R. Mecanique **337**, 48–52 (2009).
[20] E. D. Fernandez-Nieto, P. Noble, and J.-P. Vila, "Shallow water equations for non-Newtonian fluids," J. Non-Newtonian Fluid Mech. **165**, 712–732 (2010).
[21] M. Amaouche, A. Djema, and H. Abderrahmane, "Film flow for power-law fluids: Modeling and linear stability," European Journal of Mechanics B/Fluids **34**, 70–84 (2012).
[22] C. Ruyer-Quil, S. Chakraborty, and B. S. Dandapat, "Wavy regime of a power-law film flow," J. Fluid Mech. **692**, 220–256 (2012).
[23] F. Rousset, S. Millet, V. Botton, and H. Ben Hadid, "Temporal stability of Carreau fluid flow down an incline," J. Fluids Eng. **129**, 913–920 (2007).
[24] K.-X. Hu, M. He, Q.-S. Chen, and R. Liu, "Linear stability of thermocapillary liquid layers of a shear-thinning fluid," Phys. Fluids **29**, 073101 (2017).
[25] I. M. R. Sadiq and R. Usha, "Long-wave instabilities in a non-Newtonian film on a nonuniformly heated incline," J. Fluid Eng. **131**, 031202 (2009).

[26] N. Bernabeu, P. Saramito, and C. Smutek, "Modelling lava flow advance using shallow-depth approximation for three-dimensional cooling of viscoplastic flows," In A. J. L. Harris, T. De Groeve, F. Garel, and S. A. Carn, editors *Detecting, Modelling and responding to effusive eruptions*, vol. 426, London, Geological Society, London, Special Publications, 40923 (2016).
[27] S. J. D. D'Alessio, J. P. Pascal, H. A. Jasmine, and K. A. Ogden, "Film flow over heated wavy inclined surfaces," J. Fluid Mech. **665**, 418–456 (2010).
[28] S. Kalliadasis, C. Ruyer-Quil, B. Scheid, and M. G. Velarde, *Falling Liquid Films* (Springer-Verlag, London, UK, 2012), pp. 1–12.
[29] L. N. Trefethen, *Spectral methods in Matlab* (SIAM, Philadelphia, 2000).
[30] V. Y. Shkadov, "Wavy flow regimes of a thin layer of viscous fluid subject to gravity," Izv. Akad. Nauk SSSP, Mekh. Zhidk Gaza **2**, 43–51 (1967).
[31] R. J. LeVeque, *Finite volume methods for hyperbolic problems* (Cambridge University Press, Cambridge, 2002).